applied sciences

MDPI

Article

Study on Low-Speed Steering Resistance Torque of Vehicles Considering Friction between Tire and Pavement

Dong Cao [1], Bin Tang [2,*], Haobin Jiang [1,2], Chenhui Yin [1], Di Zhang [1] and Yingqiu Huang [1]

[1] School of Automotive and Traffic Engineering, Jiangsu University, Zhenjiang 212013, China; caodong.mail@foxmail.com (D.C.); jianghb@ujs.edu.cn (H.J.); 2211604077@stmail.ujs.edu.cn (C.Y.); 2211704069@stmail.ujs.edu.cn (D.Z.); huangyingqiou@foxmail.com (Y.H.)

[2] Automotive Engineering Research Institute, Jiangsu University, Zhenjiang 212013, China

* Correspondence: tangbin@ujs.edu.cn; Tel.: +86-0511-8878-2845

Received: 25 December 2018; Accepted: 7 March 2019; Published: 12 March 2019

Abstract: Electric power steering (EPS) systems under existing vehicle power systems cannot provide enough power for heavy-duty commercial vehicles under pivot or low-speed steering conditions. To solve this problem, the paper proposes an EPS system that is based on the hybrid power system constituted by the vehicle power system and the supercapacitor in parallel. In order to provide a theoretical basis for the intervention and withdrawal mechanisms of a super-capacitor in the new EPS, the law of steering resistance torque at a low or extremely low vehicle speed should be explored. Firstly, the finite element model of tire/pavement was established to conduct the simulation and calculation of the low-speed steering friction force between the tire and pavement, and to obtain the fitting expression of the equivalent steering friction coefficient with the running speed of the tire. Secondly, the expression of the steering friction torque was deduced based on the calculus theory and mathematical model of the low-speed steering resistance torque, including the steering friction torque and aligning torques, established to conduct the simulation of the equivalent resistance torque applied on a steering column under low-speed condition. Subsequently, the real vehicle experiments were carried out and comparisons of the experimental results and simulation results was performed. The consistency indicated that the model of low-speed steering resistance torque had a high accuracy. Finally, the law of low-speed steering resistance torque with a vehicle speed and steering wheel angle were analyzed according to the 3D surface plot drawn from the simulation results.

Keywords: heavy-duty commercial vehicle; electric power steering system; hybrid power system; steering resistance torque; steering friction force; aligning torque

1. Introduction

With the rapid development of China's national economy and advanced highway networks, the driving speed of heavy-duty commercial vehicles, such as coaches and lorries, has greatly increased, while high-speed safety has becoming increasingly prominent. The steering system as a key part in vehicle chassis is crucial for the driving safety of vehicles.

Nowadays, heavy-duty commercial vehicles are widely equipped with a hydraulic power steering (HPS) system, with an assist characteristic that is relatively single and an assist effort cannot vary with vehicle speed, which would easily cause poor road feel and affect handling stability during high-speed steering. On the other hand, whether the vehicle is going straight or steering, the steering pump in HPS is always running along with the engine, which causes a large amount of energy loss [1,2]. Recently, the electric power steering (EPS) system has been widely used in passenger cars and light commercial vehicles for its advantages of safety, energy saving and environmental protection. The assist effort

of EPS can vary with vehicle speed, which is conducive to improving handling stability. In addition, the motor in EPS provide steering assist effort directly, thus EPS hardly consumes electric energy under no-steering conditions, which is more energy saving [3,4]. Nevertheless, EPS is not suitable for heavy-duty commercial vehicles due to a large steering resistance torque and the power limitation of existing power supply systems in heavy-duty commercial vehicles, especially under the condition of pivot or low-speed steering [5]. It is known that heavy-duty commercial vehicles travel at medium or high speeds most of the time. In this case, the steering resistance torque is lower and the power supply system can meet the steering power demand. So the issue of insufficient power provided by existing vehicle power systems during pivot or low-speed steering needs to be emphatically solved to promote the application of EPS in heavy-duty commercial vehicles.

Supercapacitors (SC) have been widely used in electric vehicles and the braking system of trains for its advantages of high power density, short charging time, large current discharge capacity, etc. [6–8] Therefore, a new type of EPS system based on the hybrid power system constituted by the vehicle power system and the supercapacitor, which is defined as SC-EPS here, is proposed in this paper. When vehicle speed is low, the vehicle power system and supercapacitor jointly provide electric power for EPS. When the vehicle speed is high, the vehicle power system solely provides electric power for EPS while charging the supercapacitor.

In order to provide a theoretical basis for the intervention and withdrawal mechanisms of a supercapacitor in the new EPS structure, the law of steering resistance torque at a low or extremely low vehicle speed needs to be explored first. In other words, the power supply modes of the SC-EPS system are determined by the change laws of the steering resistance torque. Domestic and foreign scholars have carried out relevant research on the compositions, calculations and influences of the steering resistance torque. The pivot steering resistance torque is related to various factors such as the front axle load, the alignment parameters and steering angle of the front wheel, the tire/pavement friction, etc. [9–12] For example, empirical formulas are usually used to calculate the pivot steering resistance torque at present [13,14], however, empirical formulas do not reflect the relationship between the steering resistance torque and the steered wheel angle. Wang, Y.C. et al. analyzed the effects of the steered wheel angle, friction coefficient, tire pressure and vertical load on the pivot steering resistance torque based on a vehicle road test [15], they also considered the contact between the tire and pavement in their research on the pivot steering resistance torque [16], however, the effect of the kingpin offset on the steering resistance torque is neglected in modeling. Zhuang, Y. et al. introduced the LuGre friction model in their research on the pivot steering resistance torque, and the parameter identification and simulation calculation was carried out [17]. Zhao, Y.X. proposed the hypothesis of gradual distribution of tire load starting from contact and friction between the tire and pavement, and calculated the pivot steering resistance torque [18]. Ma, B. et al. proposed an estimation method of the static steering torque including the tire sliding torque and gravity aligning torque [19]. For the steering resistance torque under a medium and high speed steering condition, it is mainly composed of aligning torques caused by the alignment parameters of the front wheel, which is related to vehicle speed, the side-slip characteristics of the tire, pneumatic trail, the alignment parameters and steering angle of the front wheel, etc. [20–22] For example, Liu, Z. et al. analyzed the effects of vehicle speeds (10 km/h, 20 km/h, 30 km/h, 40 km/h, 50 km/h) on the steering torque based on modeling and simulation [23]. Kim, S.H. et al. took the tire lateral force, the aligning torques due to kingpin inclination and the pneumatic trail into account in their research on hardware-in-the-loop simulations of an electrohydraulic power steering system [24]. Wei, Y.T. et al. analyzed the relationships between the lateral force, the aligning torques of the tire and side-slip angle, the tire's rolling speed by establishing the simulation model of a rolling tire, and presented the change curve of the steering torque [25]. To sum up, domestic and foreign scholars mainly studied the steering resistance torque under pivot steering and medium or high speed steering conditions, but did not involve their research on low-speed steering resistance torque. According to analysis, the low-speed steering resistance torque mainly includes the tire/pavement friction torque and aligning torques caused by the alignment parameters of the front wheel. When the

vehicle steers at a low speed, the friction generated between the tire and pavement includes the components of sliding and rolling friction. The proportion of the two friction components will transfer to each other as the vehicle speed changes, and thus the dynamic process is quite complex. There are no mature models to describe such dynamic processes so far. Judging from the above gap analysis, the study on low-speed steering resistance torque not only can provides a theoretical basis for the intervention and withdrawal mechanisms of a supercapacitor in SC-EPS, but can fill in the blank in the research field on low-speed steering resistance torque, providing a useful reference for the design of assist characteristics and control strategies for other new EPS systems as well.

Considering that the low-speed steering resistance torque of heavy-duty commercial vehicles is not convenient for experimental verification, the model of low-speed steering resistance torque of a compact car was established and verified by real vehicle experiments in this paper. Then the proved modeling method of low-speed steering resistance torque would be generalized to heavy-duty commercial vehicles. Firstly, the finite element models of the tire and pavement were established to conduct the simulation and calculation of a low-speed steering friction force between the tire and pavement and to obtain the fitting expression of the equivalent steering friction coefficient with the running speed of the tire. Subsequently, the mathematical model of low-speed steering resistance torque including the steering friction torque and aligning torques were established to conduct the simulation of the equivalent resistance torque applied on a steering column in vehicle speeds of 0 km/h, 1 km/h, 2 km/h, 3 km/h, 4 km/h, 5 km/h, 10 km/h and 20 km/h, respectively, which are verified by real vehicle experiments. Finally, the law of low-speed steering resistance torque with vehicle speed and steering wheel angle was analyzed according to the 3D surface plot drawn from simulation results.

2. Structure and Working Principles of the SC-EPS System

The structure of the SC-EPS system is shown in Figure 1, including the torque/angle sensor, recirculating ball steering gear, assist motor, controller, DC–DC converter and supercapacitor. The supercapacitor was connected in parallel with the vehicle power system through the DC–DC converter to form the hybrid power system.

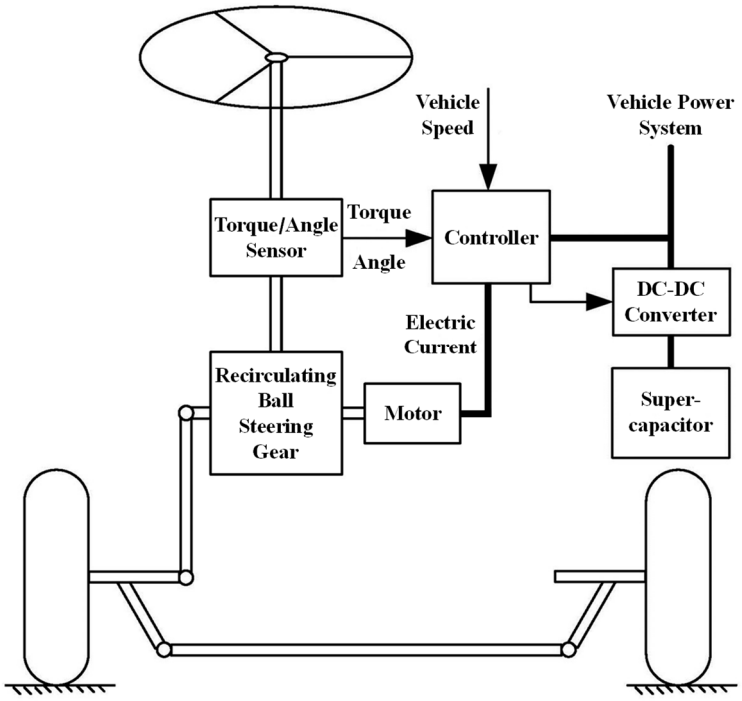

Figure 1. Structure of the SC-EPS system.

The SC-EPS system has three power supply modes: Hybrid power supply mode, vehicle power supply mode and supercapacitor power supply mode. When the vehicle speed is low, the SC-EPS system is in hybrid power supply mode. In this case, the vehicle power system and supercapacitor jointly provided electric power to the assist motor, the controller determines the mode and proportion of power distribution according to the signals, such as the vehicle speed and steering wheel angle. When the vehicle speed is high, the SC-EPS system is in vehicle power supply mode, which means the vehicle power system solely provides electric power to the assist motor. Meanwhile, the supercapacitor is in charging state to ensure that the stored energy can be used during low-speed steering. When the vehicle power system fails, the SC-EPS system is in supercapacitor power supply mode, under which the supercapacitor emergently provides electric power to the assist motor to maintain the steering assist for a short time.

3. Simulation of Low-Speed Steering Friction Force between the Tire and Pavement

In this section, the finite element models of tire and pavement based on ABAQUS software are established to carry out the simulation and calculation of steering friction force under a low-speed steering condition. The law of steering friction force with running speed of tire is explored.

The focus of this section is to study the friction between two surfaces, therefore, a few simplified treatments are made in tire modeling to reduce the difficulty of software calculation: The lateral tread pattern is ignored and only the longitudinal tread pattern is retained; the internal complex structure of tire is ignored and only the tread, carcass, cord layer and belt layer of the tire are retained; moreover, the rim would constrain the tire's deformation and should not be ignored, which is simplified into a flat-bottomed steel ring with a regular shape and assembled with the tire.

Since the rubber material, which makes up the tire tread, has extremely complex characteristics, it is usually defined as the isotropic, incompressible and hyper-elastic material in the model. The Mooney–Rivlin material model is used in this section to describe the constitution of rubber and the material parameters of each component, as shown in Table 1 [26,27]. When modeling, the steel wires of the cord layer and belt layer are simulated by a rebar unit, which is firstly defined on the surface unit and then embedded into the corresponding entity unit of rubber. The tread and carcass of the tire are constrained by a tie. The rim, which is not deformed, is rigidly coupled with the central point of carcass' rotation axis, thus it can move with the tire carcass. The finite element models of the tire and pavement are shown in Figure 2. To clarify, the kingpin inclination and caster are usually not considered in 3D finite element models to simplify the models and facilitate calculation, and the tire just rolls and deflects around the central point which is coupled with the periphery of the rim.

Table 1. Material properties of the tire and pavement.

Part	Elasticity Modulus (MPa)	Poisson's Ratio	Density (g/cm^3)	Mooney Coefficients (MPa)	
				C_{10}	C_{01}
Tread	——	——	1.14	2.0477	1.1859
Carcass	794	0.45	1.39	——	——
Belt	55,000	0.3	7.64	——	——
Pavement	1400	0.35	2.4	——	——

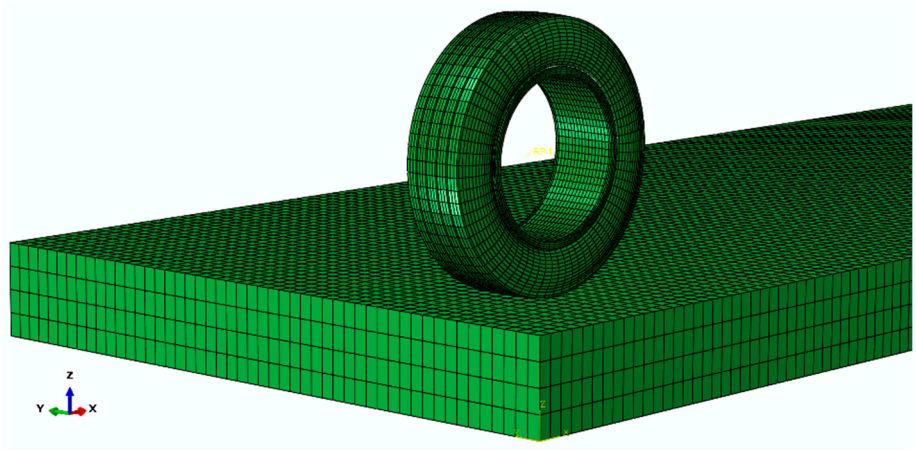

Figure 2. Finite element models of the tire and pavement.

In the simulation of low-speed steering friction, the tire pressure was set as 0.25 MPa, the vertical load on the tire was set as 3000 N and the friction coefficient of surface-to-surface contact was taken as 0.7, which is the initial value set in the software, indicating the contact property between two surfaces. The steered process of the tire was simulated by the tire's forward rolling and the pavement's horizontal tuning, respectively.

The simulations were respectively performed in tire running speeds of 1 km/h, 2 km/h, 4 km/h, 6 km/h, 8 km/h and 10 km/h. The first 3 simulation results of the steering friction force are shown in Figure 3a. It can be seen that the friction force at each speed rose gradually and then kept a steady state. The steering friction force in the steady state was averaged in all simulation results, and then the average value was treated as the steering friction force at each corresponding speed as shown in Table 2. It can be seen that the steering friction force obviously decreased with the running speed of the tire.

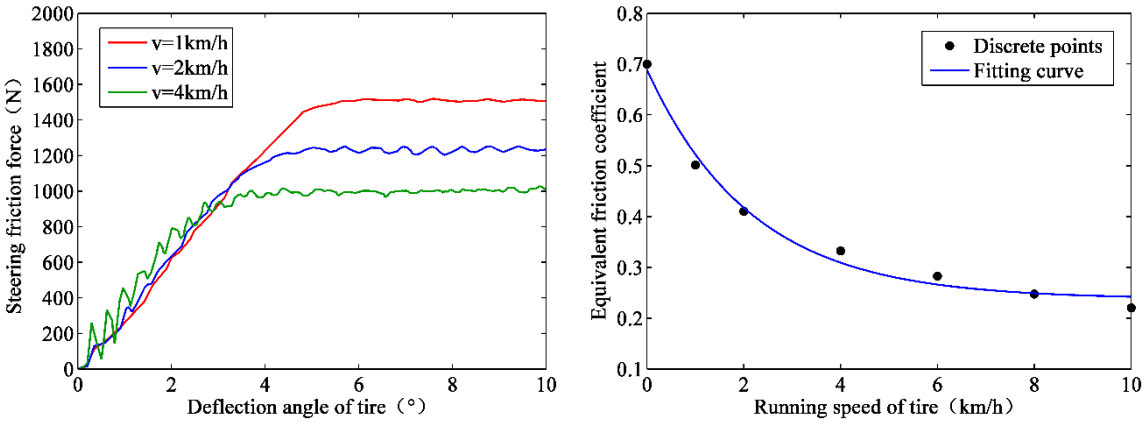

Figure 3. Simulation results of low-speed steering friction force: (**a**) Curves of steering friction force; and (**b**) fitting curve of the equivalent friction coefficient with the running speed of the tire.

Table 2. Simulation results of low-speed steering friction force.

Running Speed *u* (km/h)	**1**	**2**	**4**	**6**	**8**	**10**
Steering friction force (N)	1504.52	1230.89	997.21	847.82	741.94	660.39
Equivalent friction coefficient μ	0.5015	0.4103	0.3324	0.2826	0.2473	0.2201

Table 2 also shows the equivalent friction coefficient at different corresponding speeds, which was obtained through dividing the steering friction force by the vertical load. Subsequently, the data in Table 2 are fit in the form of $y = a \cdot e^{b \cdot x} + c$ (a, b, c are the fitting coefficients) [28], according to the variation trend and the fitting curve, which is shown in Figure 3b. Finally, the function of the equivalent friction coefficient with running speed is:

$$\mu = f(u) = 0.4511 \cdot e^{-0.4603 \cdot u} + 0.2376 \tag{1}$$

where μ is the equivalent friction coefficient between the tire and pavement under a low-speed steering condition; u is the running speed of the tire, km/h.

The value of μ in Equation (1) can be treated as the friction coefficient between the tire and pavement under pivot steering condition when $u = 0$, which is consistent with the value of f in the commonly used empirical formula of the pivot steering resistance torque [13].

4. Modeling of Low-Speed Steering Resistance Torque Considering Tire/Pavement Friction

On the premise that the friction inside the steering system itself is ignored, the steering resistance torque mainly consists of 4 parts under a low-speed steering condition: The low-speed steering friction torque and aligning torques caused by the kingpin inclination, kingpin caster and pneumatic trail.

4.1. Low-Speed Steering Friction Torque between the Tire and Pavement

There is surface contact between the tire and pavement, as shown in Figure 4. Where δ_t is the deformation or subsidence of the tire, l_t and b_t are respectively the length and width of the tire/pavement contact region. The values of δ_t, l_t and b_t can be calculated by the following empirical formulas [29]:

$$\delta_t = c_t k_t \frac{F_z^{0.85}}{B^{0.7} D^{0.43} P^{0.6}} \tag{2}$$

$$l_t = 2D\left(\frac{\delta_t}{D}\right)^s \tag{3}$$

$$b_t = B\left(1 - e^{-t\delta_t}\right) \tag{4}$$

where c_t is the parameter related to the tire type, $c_t = 1.15$ for bias tires and $c_t = 1.5$ for radial tires, $k_t = 0.015B + 0.42$, F_z is the vertical load on the tire with the unit of 10 N, B is the width of tire with the unit of cm, D is the diameter of the tire with the unit of cm, P is the tire pressure with the unit of 100 kPa and s and t are the empirical coefficients, which are 0.557 and 122.7 respectively.

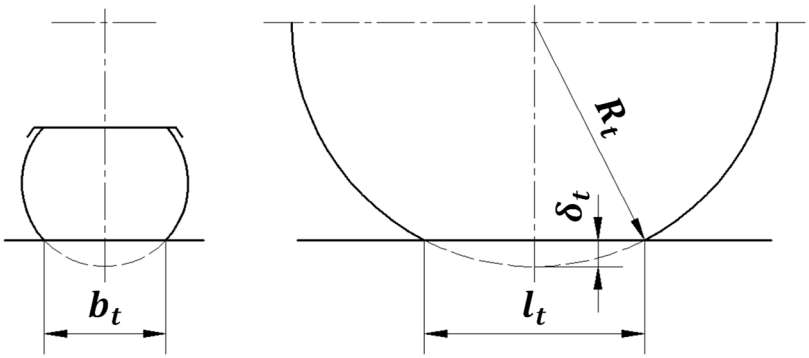

Figure 4. Diagram of contact between the tire and pavement.

It is known that the steered wheel does not turn around the center of the tire/pavement contact region rather than around the kingpin axis when the vehicle is steering. There is a certain distance between the intersection of the kingpin axis to the pavement and the center of the contact region,

which is called the kingpin offset, as shown in Figure 5a. On the other hand, when the pressure is constant, the tire with a low load has a circular shape near the contact region center. As the load increases, the tire will come into contact with the pavement over the entire width, and the contact region shape will become approximately elliptical and rectangular. Therefore, the shape of the contact region is taken as a rectangle for investigation in this paper. Considering the influence of the kingpin offset on the steering resistance torque, the geometric model of the low-speed steering friction torque between the tire and pavement is established in the coordinate system with the intersection of the kingpin axis to the pavement as origin, as shown in Figure 5b.

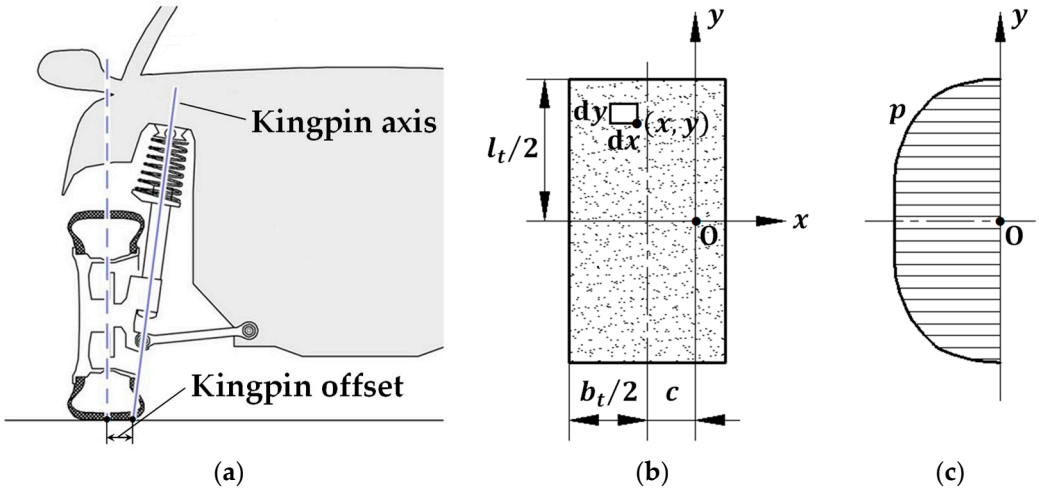

Figure 5. Steering model of the steered wheel: (**a**) Schematic diagram of the kingpin axis and kingpin offset; (**b**) geometric model of the low-speed steering friction torque; and (**c**) longitudinal pressure distribution of the tire.

Figure 5c shows the corresponding longitudinal pressure distribution of the tire, and the expression is shown as follows:

$$p(x,y) = \frac{n+1}{n}\frac{2^n F_z}{{l_t}^{n+1} b_t}\left[\left(\frac{l_t}{2}\right)^n - y^n\right] \tag{5}$$

where n is a constant, $n = 2$~10 in general, which can be approximately $n = 4$ for the radial tire.

In Figure 5b, an infinitesimal element with dx as length and dy as width at an arbitrary point (x, y) is taken in the tire/pavement contact region, as a consequence, the load on the infinitesimal element is:

$$\mathrm{d}F_z = p(x,y) \cdot \mathrm{d}x \cdot \mathrm{d}y \tag{6}$$

When the infinitesimal element rotates around the original point O on the pavement, the friction force between the two is:

$$\mathrm{d}F_f = \mu \cdot \mathrm{d}F_z = \mu \cdot p(x,y) \cdot \mathrm{d}x \cdot \mathrm{d}y \tag{7}$$

where μ is the friction coefficient between the tire and pavement.

Since the distance from this arbitrary point (x, y) to point O is $r = \sqrt{x^2 + y^2}$, the friction torque of the infinitesimal element to point O is:

$$\mathrm{d}M_f = r \cdot \mathrm{d}F_f = \sqrt{x^2 + y^2} \cdot \mu \cdot p(x,y) \cdot \mathrm{d}x \cdot \mathrm{d}y \tag{8}$$

The steering friction torque of a single tire can be calculated by integrating $\mathrm{d}M_f$ on the whole contact region, which is denoted as M_{f-s} and can be expressed as:

$$M_{f-s} = \iint_S \mathrm{d}M_f = \int_{-(\frac{b_t}{2}+c)}^{(\frac{b_t}{2}-c)} \mathrm{d}x \int_{-\frac{l_t}{2}}^{\frac{l_t}{2}} \mu p(x,y) \sqrt{x^2+y^2} \mathrm{d}y \tag{9}$$

where c is the kingpin offset.

Under a low-speed steering condition, the friction coefficient μ between the tire and pavement can be represented approximately by Equation (1). Considering the direction of the steering friction torque, the expression of the low-speed steering friction torque can be finally written as:

$$\begin{cases} M_f = -\mathrm{sign}\left(\frac{\mathrm{d}\delta}{\mathrm{d}t}\right) \cdot 2 \cdot M_{f-s} = -\mathrm{sign}\left(\frac{\mathrm{d}\delta}{\mathrm{d}t}\right) \cdot 2 \cdot \int_{-(\frac{b_t}{2}+c)}^{(\frac{b_t}{2}-c)} \mathrm{d}x \int_{-\frac{l_t}{2}}^{\frac{l_t}{2}} \mu p(x,y) \sqrt{x^2+y^2} \mathrm{d}y \\ \mu = f(u) = 0.4511 \cdot e^{-0.4603 \cdot u} + 0.2376 \\ p(x,y) = \frac{5}{4} \frac{2^4 F_z}{l_t^5 b_t} \left[\left(\frac{l_t}{2}\right)^4 - y^4 \right] \end{cases} \tag{10}$$

where M_f is the low-speed steering friction torque, δ is the steered wheel angle, "$-\mathrm{sign}\left(\frac{\mathrm{d}\delta}{\mathrm{d}t}\right)$", which indicates that the direction of M_f is always opposite to the turning direction of the steered wheel and u is the vehicle speed.

When $u = 0$, the value of M_f in Equation (10) can be regarded as the friction torque under the pivot steering condition.

4.2. The Aligning Torque Caused by the Kingpin Inclination

The existence of the kingpin inclination makes the steering system work against the front axle load when steering and makes the steered wheel return to the center automatically as well [30]. The corresponding aligning torque can be expressed as:

$$M_\theta = -G_1 \cdot \left[c + \left(\frac{D}{2} - \delta_t \right) \tan\theta \right] \cdot \sin(2\theta) \cdot \sin\left(\frac{\delta}{2}\right) \tag{11}$$

where θ is the kingpin inclination angle, M_θ is the aligning torque caused by the kingpin inclination, "$-$" indicates that the direction of M_θ is always opposite to the direction of steered wheel angle, G_1 is the front axle load and c is the kingpin offset.

4.3. Aligning Torques Caused by the Kingpin Caster and Pneumatic Trail

Due to the centrifugal effect, the lateral force F_y exists at the center of steered wheel when the vehicle steers. Accordingly, the lateral reaction force F_Y, which is also known as the cornering force, is generated by the pavement on the steered wheel. The cornering force produces the aligning torques which is related to the kingpin caster trail and pneumatic trail. The detailed solution procedure of the aligning torques caused by the kingpin caster and pneumatic trail is shown in Figure 6. The 2-degree-of-freedom (2-dof) vehicle dynamic model is employed here to calculate the ideal side-slip angle and yaw rate. It can also be used to identify and estimate the actual side-slip angle. Under the 2-dof vehicle model, the lateral force and the aligning torque are considered acting on the front axle as a whole, which is consistent with the processing ideas in the calculation of M_f and M_θ in Sections 4.1 and 4.2.

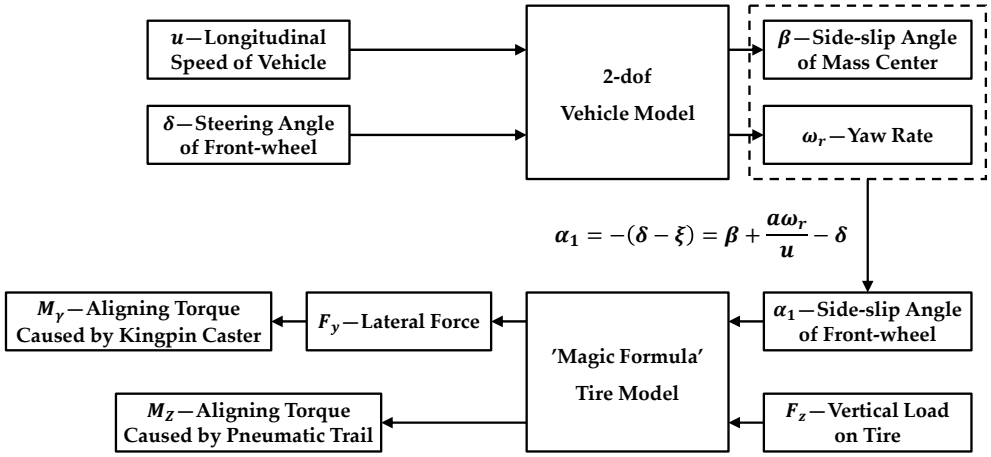

Figure 6. Solution procedure of the aligning torques caused by the kingpin caster and pneumatic trail.

The corresponding vehicle motion differential equations of the 2-dof vehicle model in Figure 6 are expressed as Equation (12) [31]:

$$\begin{cases} (k_1 + k_2)\beta + \frac{1}{u}(ak_1 - bk_2)\omega_r - k_1\delta = m(\dot{v} + u\omega_r) \\ (ak_1 - bk_2)\beta + \frac{1}{u}(a^2k_1 + b^2k_2)\omega_r - ak_1\delta = I_Z\dot{\omega}_r \end{cases} \tag{12}$$

where a and b are respectively the distance from the front and rear axle to the center of mass, k_1 and k_2 are respectively the cornering stiffness of the front and rear wheel, u and v are respectively the longitudinal velocity along the x-axis and the lateral velocity along the y-axis of the vehicle, I_Z is the rotational inertia around the z-axis, β is the side-slip angle of the mass center, ω_r is the yaw rate and δ is the steered wheel angle.

According to the 2-dof vehicle motion differential equations in Equation (12), the simulation model is established in the MATLAB/Simulink environment, which takes the forward velocity u and steered wheel angle δ as input, and takes the side-slip angle of mass center β and yaw rate ω_r as output. The desired side-slip angle of the front wheel α_1 can be obtained by one more step calculation, which is:

$$\alpha_1 = -(\delta - \xi) = \beta + \frac{a\omega_r}{u} - \delta \tag{13}$$

When the vehicle is steering, the tire easily gets into a nonlinear state. Combined with the side-slip angle of the tire and vertical load, the 'Magic Formula' tire model is used to calculate the lateral force F_y and aligning torque caused by the pneumatic trail M_Z, so as to accurately describe the mechanical characteristics of the tire. The expressions of the lateral force F_y and aligning torque M_Z are as follows [32]:

$$\begin{cases} F_y = D_1 \sin\{C_1 \arctan[B_1(1 - E_1)\alpha + E_1 \arctan(B_1\alpha)]\} \\ M_Z = D_2 \sin\{C_2 \arctan[B_2(1 - E_2)\alpha + E_2 \arctan(B_2\alpha)]\} \end{cases} \tag{14}$$

where D_1, B_1, C_1 and E_1 are respectively the peak factor, stiffness factor, shape factor and curvature factor for the solution of lateral force. D_2, B_2, C_2 and E_2 are respectively the peak factor, stiffness factor, shape factor and curvature factor for the solution of the aligning torque and α is the side-slip angle of the tire.

Under a single steering condition, the coefficients of the 'Magic Formula' can be referred to in the literature [33]. The curves of the lateral force F_y and the aligning torque caused by the pneumatic trail M_Z with the side-slip angle of the tire α are drawn according to Equation (14) in the MATLAB, which are shown in Figure 7a,b.

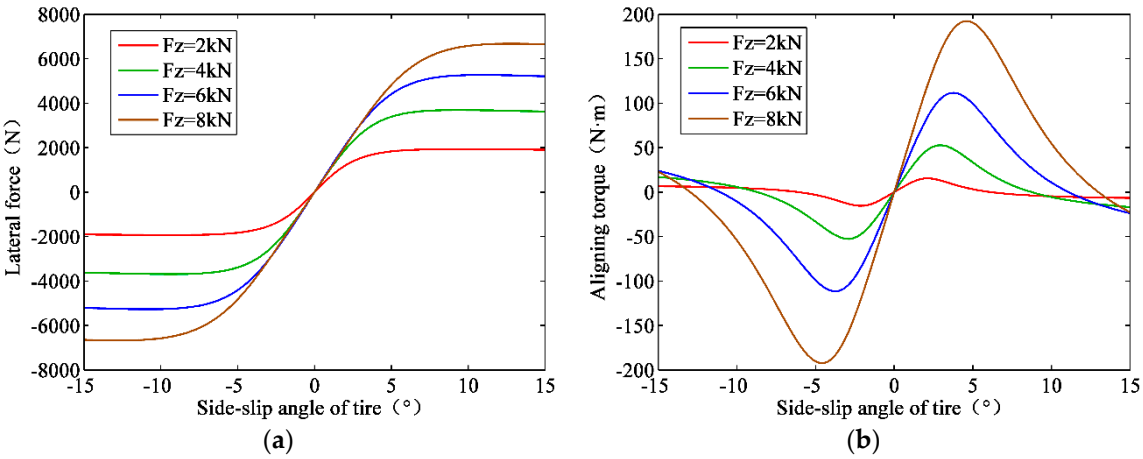

Figure 7. The relation curves obtained by 'Magic Formula': (**a**) The lateral force with the side-slip angle of tire; and (**b**) the aligning torque with the side-slip angle of tire.

Furthermore, the aligning torque caused by the kingpin caster can be expressed as:

$$M_\gamma = -F_Y \cdot l = F_y \cdot l = F_y \cdot \frac{D}{2} \sin\gamma \cos\delta \tag{15}$$

where γ is the kingpin caster angle, "$-$" indicates that the direction of M_γ is opposite to the direction of F_Y and l is the distance from the contact point of the steered wheel and pavement to the kingpin axis in the vehicle's longitudinal plane.

4.4. Model of the Low-Speed Steering Resistance Torque

Since the components of the steering resistance torque have taken into account directions in their equations, they just need to be added up. The low-speed steering resistance torque is equal to the sum of the low-speed steering friction torque between the tire/pavement and the aligning torques caused by the kingpin inclination, kingpin caster and pneumatic trail, as shown in Equation (16):

$$M_r = M_f + M_\theta + M_\gamma + M_Z \tag{16}$$

In the case of pivot steering, only the aligning torque caused by the kingpin inclination needs to be considered in the calculation of the aligning torque.

5. Model Simulation and Validation by Experiments

5.1. Model Simulation

The simulation models of the pivot and low-speed steering resistance torque are respectively established in the MATLAB/Simulink environment according to Equation (16). In the simulation models, the input signal is the steering wheel angle which is simulated by a periodic signal of triangular wave, and the output signal is the equivalent resistance torque applied on the steering column. Moreover, the equivalent resistance torque on the steering column and steering resistance torque have the following relations:

$$T_r = \frac{M_r}{i_{\omega 0} \cdot \eta_+} \tag{17}$$

where T_r is the equivalent resistance torque on the steering column, M_r is the steering resistance torque, $i_{\omega 0}$ is the angle ratio of the steering system and η_+ is the forward efficiency of the steering gear.

The simulation model of the low-speed steering resistance torque is shown in Figure 8.

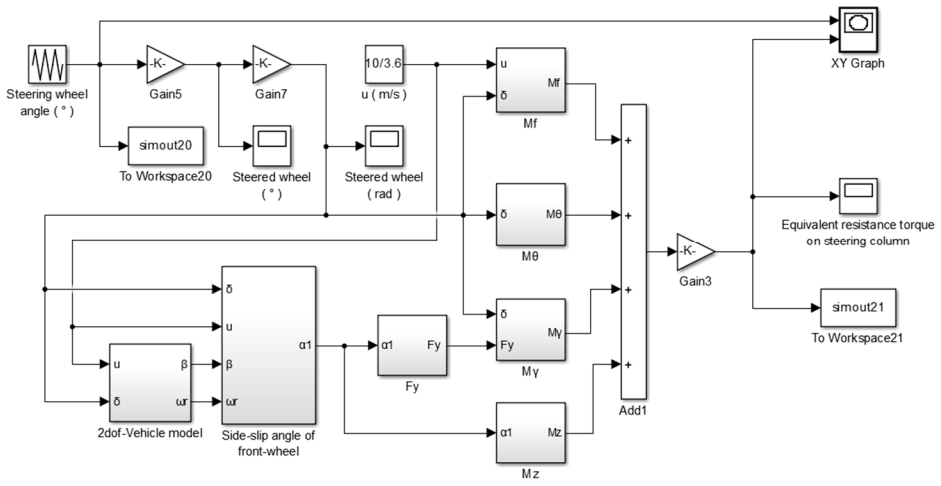

Figure 8. Simulation model of the low-speed steering resistance torque.

5.2. Real Vehicle Experiments

Taking a compact car as the test object, the experiments of the pivot and low-speed steering resistance torque were carried out.

The experimental apparatus mainly included the MSW DTI sensor-Universal measurement steering wheel and the Correvit S-Motion DTI Non-contact optical sensor. Detailed information on the main experimental apparatus is shown in Table 3. When the driver turned the measurement steering wheel, which is tightly mounted on the vehicle steering wheel through brackets, the real-time steering wheel torque/angle could be measured. The Correvit S-Motion DTI Non-contact optical sensor was fixed on the vehicle door by suckers. After relevant parameters were configured, the real-time vehicle speed, lateral acceleration and yaw rate could be measured in the process of vehicle movement. The experimental apparatus was connected to the power supply and the notebook computer, and all the measured data were recorded by DEWESoft software in the computer.

Table 3. Detailed information of main experimental apparatus.

Apparatus	Application	Type	Manufacturer
MSW DTI sensor Universal measurement steering wheel	Universal measurement steering wheel for measurement of the steering torque, steering angle and steering speed; for vehicle driving dynamics tests like ISO 4138, steady-state circular course drive.	5612A	KISTLER
Correvit S-Motion DTI Non-contact optical sensor	High-precision, slip-free measurement of: • Distance; • Speed (*x*,*y*); • Acceleration and angular rates; • GPS position data and time; • Pitch and roll angle.	2055A	KISTLER

Before the experiments, the assist power of vehicle steering system needed to be cut off. The experimental procedures were as follows: Make the vehicle respectively maintain a static state and uniform linear motion state at different speeds (1 km/h, 2 km/h, 3 km/h, 4 km/h, 5 km/h, 10 km/h, 15 km/h and 20 km/h), turn the measurement steering wheel to the left and right with a constant

speed and then collect the data of the steering wheel torque/angle, vehicle speed as well as the lateral acceleration and yaw rate of the vehicle, and then conduct several experiments for each condition.

The experimental scene is shown in Figure 9.

Figure 9. The experimental scene.

5.3. Comparison of Simulation and Experiment Results

On the premise of no steering assist power, it can be known from Newton's Third Law that the steering wheel torque and equivalent resistance torque on the steering column are equal and opposite in direction when turning the steering wheel at a constant speed, as shown in Equation (18):

$$T_s = -T_r = -\frac{M_r}{i_{\omega 0} \cdot \eta_+} \tag{18}$$

where T_s is the steering wheel torque and T_r is the equivalent resistance torque on the steering column.

Thus, the measured steering wheel torque and the simulated equivalent resistance torque on the steering column can be contrasted to verify the accuracy of the low-speed steering resistance torque model. The comparative results are shown in Figure 10. For the pivot steering experiment, the driver turned the measurement steering wheel with a constant speed when the vehicle was under a static state, causing the steering wheel to reach the limit positions on two sides. As a result, there are two mutations on the curve in Figure 10a. For the low-speed steering experiments, the driver turned the measurement steering wheel when the vehicle maintained a state of uniform linear motion at different speeds (1 km/h, 2 km/h, 3 km/h, 4 km/h, 5 km/h, 10 km/h, 15 km/h and 20 km/h). The steering wheel did not reach the limit position on either side for safety. Therefore, it is round at the corner of the curves from Figure 10b–h. In addition, the decreasing height of these curve rings from Figure 10a–h, which means the steering resistance torque decreases with the vehicle speed. It can be seen from the figures that the simulation results are consistent with the experimental results, indicating that the established model of the steering resistance torque has a high accuracy.

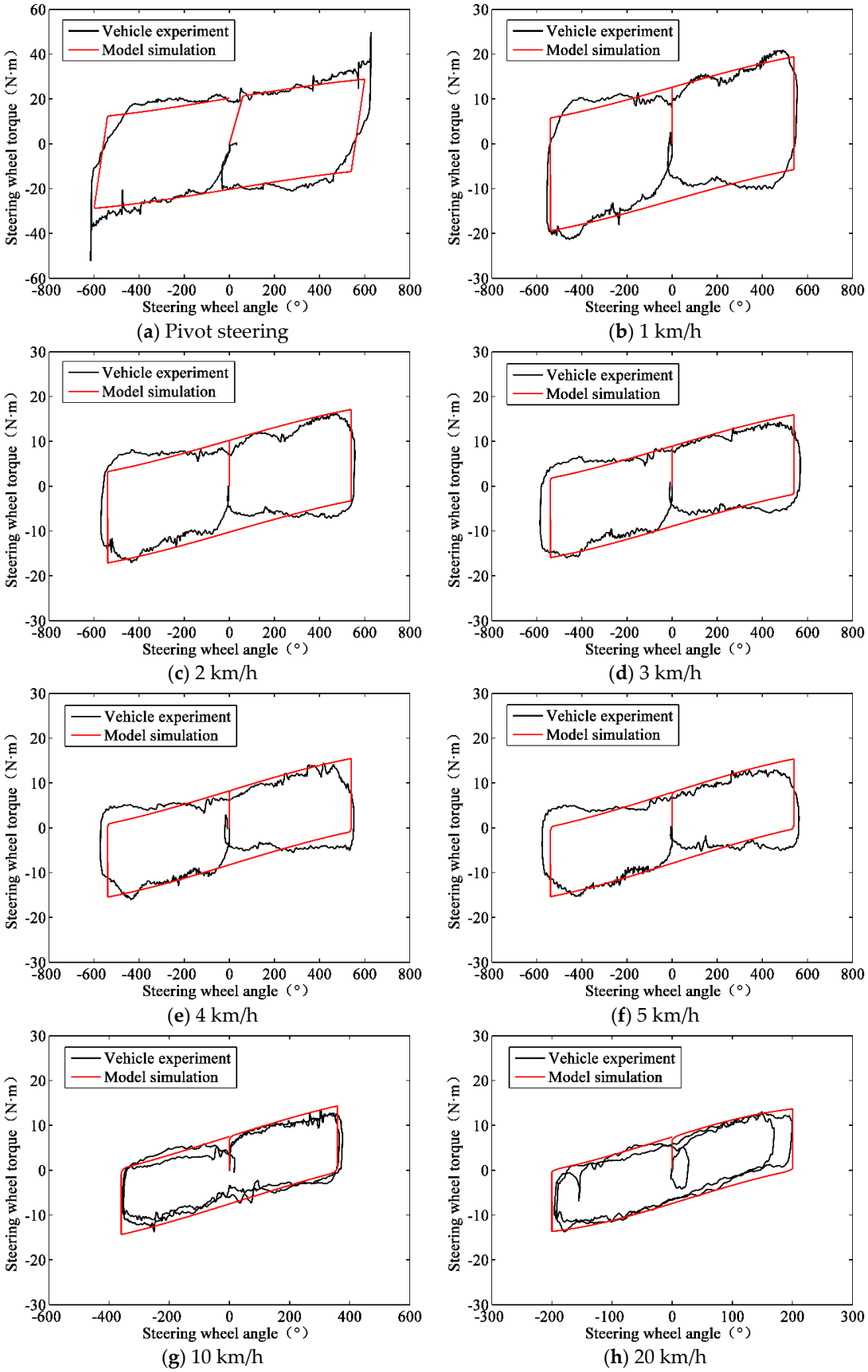

Figure 10. Simulation and experimental results of the steering wheel torque at different speeds.

Furthermore, the surface plot of the low-speed steering resistance torque with the vehicle speed and steering wheel angle can be finally drawn based on the simulation results, as shown in Figure 11. It can be clearly seen from the figure that the change laws of the low-speed steering resistance torque are as follows:

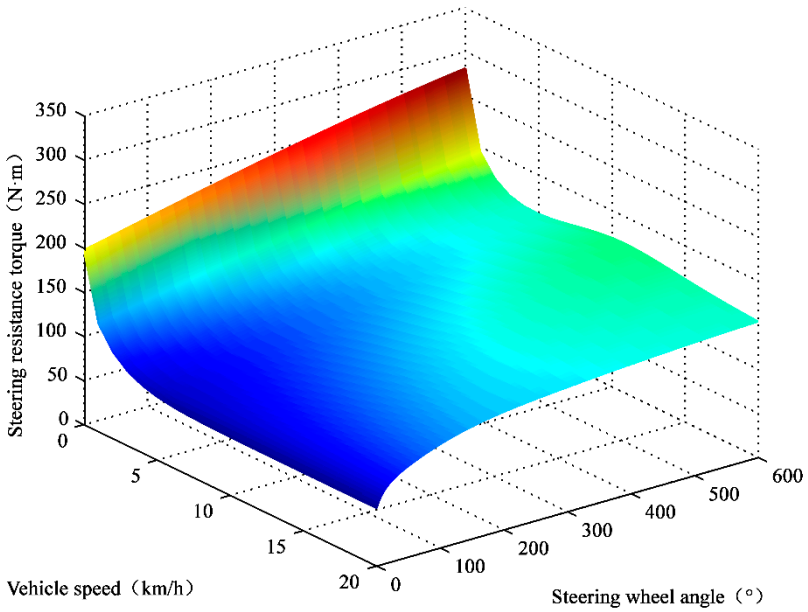

Figure 11. 3D surface plot of the low-speed steering resistance torque.

1. The low-speed steering resistance torque increased with the steering wheel angle at a certain speed. When the vehicle speed was below 10 km/h, the steering resistance torque almost changed linearly with the steering wheel angle. When the vehicle speed was between 10 km/h and 20 km/h, the steering resistance torque varied nonlinearly with the steering wheel angle;

2. The low-speed steering resistance torque decreased with the vehicle speed at a certain steering wheel angle. When the vehicle speed was in the range of 0 km/h to 5 km/h, the steering resistance torque decreased rapidly with the vehicle speed. When the vehicle speed exceeded 5 km/h, the change of the steering resistance torque was not obvious.

6. Conclusions

The steering wheel angle and the vehicle speed had great effects on the steering resistance torque. The study on low-speed steering resistance torque can provide a theoretical basis for the intervention and withdrawal mechanisms of a supercapacitor in the SC-EPS system on the one hand, and the fill the gap in the research field on low-speed steering resistance torque on the other hand, providing a useful reference for the design of assist characteristics and control strategies for other new EPS systems.

The work done in this paper and the results found from the above analyses have all come to the following conclusions:

1. The finite element (FE) model of steering friction force between the tire and pavement was established and the exponential expression of the equivalent steering friction coefficient with the vehicle speed was obtained by means of FE simulation and numerical fitting;

2. The expression of the steering friction torque between the tire and pavement was derived based on calculus theory. The mathematical model of the low-speed steering resistance torque including the steering friction torque and aligning torques was constructed, and the accuracy of the model was verified by real vehicle experiments;

3. The low-speed steering resistance torque increased with the steering wheel angle at a certain vehicle speed. As the vehicle speed increased, the low-speed steering resistance torque gradually presented nonlinearity with the steering wheel angle;

4. The low-speed steering resistance torque decreased with the vehicle speed at a certain steering wheel angle. When vehicle speed was below 5 km/h, the steering resistance torque significantly dropped off. When vehicle speed was above 5 km/h, the rate of decrease slowed down gradually.

Author Contributions: D.C. and B.T. conceived of and designed the method. D.C., C.Y., D.Z. and Y.H. performed the experiments and analyzed the experimental data. Finally, D.C. wrote the paper under the guidance of H.J. and B.T.

Funding: The work in this paper is supported by National Natural Science Foundation of China (Grant No. 51605199, No. 51675235), Natural Science Foundation of Jiangsu Province (Grant No. BK20160527), China Postdoctoral Science Foundation (Grant No. 2016M590417), Natural Science Foundation for Colleges and Universities of Jiangsu Province (Grant No. 16KJB580001) and Jiangsu Province Postdoctoral Science Foundation (Grant No. 1601222C).

Acknowledgments: The authors would like to thank the teachers in the laboratory for their guidance on the use of the experimental apparatus, and Jiangsu Gang Yang Steering Gear Company for providing the experimental site. Meanwhile, many thanks to Chen Zhu, Ziyan Lin and Yue Yin for participating in the experiments, as well as other teachers and students in the research group for participating in the discussion.

Conflicts of Interest: The authors declare no conflict of interest.

References

1. Tang, B.; Jiang, H.B.; Xu, Z.; Geng, G.; Xu, X. Dynamics of electromagnetic slip coupling for hydraulic power steering application and its energy-saving characteristics. *J. Cent. South Univ.* **2015**, *22*, 1994–2000. [CrossRef]
2. Tang, B.; Jiang, H.B.; Gong, X.Q. Optimal design of variable assist characteristics of electronically controlled hydraulic power steering system based on simulated annealing particle swarm optimisation algorithm. *Int. J. Veh. Des.* **2017**, *73*, 189–207. [CrossRef]
3. Hanifah, R.A.; Toha, S.F.; Ahmad, S.; Hassan, M.K. Swarm-Intelligence Tuned Current Reduction for Power-Assisted Steering Control in Electric Vehicles. *IEEE Trans. Ind. Electron.* **2018**, *65*, 7202–7210. [CrossRef]
4. Du, P.P.; Su, H.; Tang, G.Y. Active Return-to-Center Control Based on Torque and Angle Sensors for Electric Power Steering Systems. *Sensors.* **2018**, *18*, 855.
5. Zhao, W.Z.; Luan, Z.K.; Wang, C.Y. Parameter optimization design of vehicle E-HHPS system based on an improved MOPSO algorithm. *Adv. Eng. Softw.* **2018**, *123*, 51–61. [CrossRef]
6. Ben Fathallah, M.A.; Ben Othman, A.; Besbes, M. Modeling a photovoltaic energy storage system based on super capacitor, simulation and evaluation of experimental performance. *Appl. Phys. A Mater. Sci. Process.* **2018**, *124*, 120. [CrossRef]
7. Haubert, T.; Mindl, P.; Cerovsky, Z. Design of Control and Switching Frequency Optimization of DC/DC Power Converter for Super-capacitor. *Automatika* **2016**, *57*, 141–149. [CrossRef]
8. Farhadi, M.; Mohammed, O.A. Event-Based Protection Scheme for a Multiterminal Hybrid DC Power System. *IEEE Trans. Smart Grid* **2015**, *6*, 1658–1669. [CrossRef]
9. Jin, Y.; LU, Y.; Gong, J.H.; Lu, Z.; Li, W.; Wu, J. Design and Experiment of Electronic-hydraulic Loading Test-bed Based on Tractor's Hydraulic Steering By-wire. *Asian Agric. Res.* **2015**, *7*, 86–89.
10. Shiiba, T.; Murata, W. Experimental validation of steering torque feedback simulator through vehicle running test. *J. Mech. Sci. Technol.* **2009**, *23*, 954–959. [CrossRef]
11. Karimi, D.; Mann, D. Torque feedback on the steering wheel of agricultural vehicles. *Comput. Electron. Agric.* **2009**, *65*, 77–84. [CrossRef]
12. Park, W.; Ho, L.C.; Lee, S.; Ssung, L.K. The Effect of Ground Condition, Tire Inflation Pressure and Axle Load on Steering Torque. *J. Biosyst. Eng.* **2004**, *29*, 419–424. [CrossRef]
13. Jiang, H.B. Variable Assist Characteristics and Control Strategies for ECHPS in Terms of Maneuverability and Energy Efficiency. *J. Mech. Eng.* **2015**, *51*, 88–97. [CrossRef]
14. Sharp, R.S.; Granger, R. On car steering torques at parking speeds. *Proc. Inst. Mech. Eng. Part D-J. Autom. Eng.* **2003**, *217*, 87–96. [CrossRef]

15. Wang, Y.C.; Gao, X.H.; Zhang, X.J. Static steering resisting moment of tire for heavy multi-axle steering vehicle. *Trans. Chin. Soc. Agric. Eng.* **2010**, *26*, 146–150.
16. Wang, Y.C.; Feng, P.F.; Pang, W.J.; Zhou, M. Pivot steering resistance torque based on tire torsion deformation. *J. Terramech.* **2014**, *52*, 47–55.
17. Zhuang, Y.; Guo, K.H. Tire Spot Turn Model Based on LuGre Model. *Autom. Technol.* **2008**, *7*, 1–2.
18. Zhao, Y.X. The Research of Steering Characteristic Based on Steering Resistance Torque. Master's Thesis, Chongqing University of Technology, Chongqing, China, June 2013.
19. Ma, B.; Yang, Y.Y.; Liu, Y.H.; Ji, X.; Zheng, H. Analysis of vehicle static steering torque based on tire-road contact patch sliding model and variable transmission ratio. *Adv. Mech. Eng.* **2016**, *8*, 1–11. [CrossRef]
20. Tamakawa, S.; Tanabe, H.; Mouri, H. Relationship between steering torque and ease of driving with bar type steering in high speed range. *J. Adv. Mech. Des. Syst. Manuf.* **2017**, *11*. [CrossRef]
21. Kim, S.H.; Chu, C.N. A new manual Steering torque estimation model for steer-by-wire systems. *Proc. Inst. Mech. Eng. Part D-J. Autom. Eng.* **2016**, *230*, 993–1008. [CrossRef]
22. Hayama, R.; Kawahara, S.; Nakano, S.; Kumamoto, H. Resistance torque control for steer-by-wire system to improve human-machine interface. *Veh. Syst. Dyn.* **2010**, *48*, 1065–1075. [CrossRef]
23. Liu, Z.; Yang, J.J.; Liao, D.X. Effects of Vehicle Speed on Steering Torque. *China Mech. Eng.* **2005**, *16*, 748–751.
24. Kim, S.H.; Chu, C.N. Hardware-in-the-loop simulations of an electrohydraulic power steering system for developing the motor speed map of heavy commercial vehicles. *Proc. Inst. Mech. Eng. Part D J. Autom. Eng.* **2015**, *229*, 1717–1731. [CrossRef]
25. Wei, Y.T.; Oertel, C.; Liu, Y.H.; Li, X. A theoretical model of speed-dependent steering torque for rolling tyres. *Veh. Syst. Dyn.* **2016**, *54*, 463–473. [CrossRef]
26. Tang, T.; Johnson, D.; Smith, R.E.; Felicellia, S.D. Numerical evaluation of the temperature field of steady-state rolling tires. *Eng. Fail. Anal.* **2014**, *38*, 1622–1637. [CrossRef]
27. Li, Y.; Liu, W.Y.; Frimpong, S. Effect of ambient temperature on stress, deformation and temperature of dump truck tire. *Mater. Des.* **2012**, *23*, 55–62. [CrossRef]
28. Zhuang, J.D. *Vehicle Tire Science*, 1st ed.; Beijing Institute of Technology Press: Beijing, China, 1996; pp. 200–209, ISBN 7-81045-067-0.
29. Zhuang, J.D. *Calculation of Vehicle Terramechanics*, 1st ed.; China Machine Press: Beijing, China, 2002; pp. 52–60, ISBN 7-111-09417-4.
30. Chen, S.A.; Qiu, F.; He, R.; Lu, S. Analysis of Self-aligning Torque from Vehicle Kingpin Inclination. *Trans. Chin. Soc. Agric. Mach.* **2008**, *39*, 32–35.
31. Jiang, Z.Z.; Xiao, B.X. LQR optimal control research for four-wheel steering forklift based-on state feedback. *J. Mech. Sci. Technol.* **2018**, *32*, 2789–2801. [CrossRef]
32. Tang, B.; Jiang, H.B.; Chen, L.; Geng, G.; Yao, J. Steering Stability Control of Vehicles Equipped with E-ECHPS Based on Differential Geometry. *Trans. Chin. Soc. Agric. Mach.* **2015**, *46*, 285–293.
33. Shi, P.C.; Zhao, Q.; Zhang, R.Y.; Li, Y. The Simulation of Tire Dynamic Performance Based on "Magic Formula". In Proceedings of the 2017 2nd International Conference on Automation, Mechanical Control and Computational Engineering (AMCCE 2017), Beijing, China, 25–26 March 2017; pp. 699–703.